Cirella Antonella (Orcid ID: 0000-0002-4144-3794)
Pezzo Giuseppe (Orcid ID: 0000-0003-4851-4193)
Piatanesi Alessio (Orcid ID: 0000-0003-2863-3662)

Rupture Kinematics and Structural - Rheological Control of the 2016 M_w6.1 Amatrice (Central Italy) Earthquake from Joint Inversion of Seismic and Geodetic Data

Cirella A.[1], G.Pezzo[1], and A. Piatanesi[1]

[1]Istituto Nazionale di Geofisica e Vulcanologia, Rome, Italy

This is the author manuscript accepted for publication and has undergone full peer review but has not been through the copyediting, typesetting, pagination and proofreading process, which may lead to differences between this version and the Version of Record. Please cite this article as doi: 10.1029/2018GL080894

Abstract

We investigate the rupture process of the 2016, M_w6.1 Amatrice earthquake, the first shock of a seismic sequence characterized by three damaging earthquakes occurred in Central Italy between August and October. We jointly invert strong motion, High-Rate GPS data, GPS and DInSAR displacements and we adopt ad-hoc velocity profiles of the crust below each station. The retrieved source model reveals a high degree of complexity, characterized by a prominent bi-lateral rupture with low slip at the hypocentre, two well-separated slip patches and a rupture front accelerating when breaking the largest patch. The rupture of the main asperity features a slip-velocity pulse that is impeded ahead of its current direction and splits into two pulses. In this fault section we find clues of structural and rheological control of the rupture propagation due to the fault system segmentation.

1. Introduction

The 2016 Amatrice earthquake (M_w 6.1) occurred in the Central Apennines (Italy) on August 24th at 01:36 UTC, causing about 300 fatalities, and heavily damaging the economy of the region. The hypocentre has been located at 13.238°E, 42.704°N, at a depth of 8.0 km (http://cnt.rm.ingv.it/event/7073641); it is the first shock of a seismic sequence characterized by three damaging earthquakes occurred in Central Italy between August and October. One hour later a M_w 5.3 aftershock had been located at 13.15°E, 42.79°N, at a depth of 8km (http://cnt.rm.ingv.it/event/7076161). On October 26th (19:18 UTC) a M_w 5.9 earthquake occurred 25km to the NW, 3km West of Visso; and few days later, on October 30th (06:40 UTC), a third major earthquake (M_w 6.5) nucleated 6km North of Norcia. The three main events show normal focal mechanisms striking NNW-SSE, in agreement with the extensional tectonic regime of the central Apennines [D'Agostino et al., 2009].

The entire 2016 Central Italy sequence extends about 60km, it involves a region bordered by the 1997 Umbria-Marche sequence to the North, and the 2009 L'Aquila earthquake to the South [Chiaraluce et al., 2017], both showing normal focal mechanisms. The epicentral area experienced: i) a Jurassic extension forming large normal faults [Butler et al., 2006; Ciarapica & Passeri, 2002]; ii) a late Miocene-early Pliocene compression creating the thrust-and-fold systems [Barchi et al., 1998a; Vezzani et al., 2010] and iii) a late Pliocene-Quaternary

extension forming the current intramountain basins [Barchi et al., 1998b; Cavinato & De Celles, 1999; Lavecchia et al., 1994]. The 24th August mainshock originated along the Mt. Gorzano Fault System (GFS) and involved the Mt. Bove - Mt. Vettore Fault System (BVFS) separated by the Sibillini Thrust Front (STF) [Centamore et al., 2009; Lavecchia, 1985], representing an evident lithological and structural discontinuity crossing the epicentral area.
In this work we achieve the following goals:

- Build-up a new fault geometry consistent with both geodetic and seismological data.
- Image the full kinematic rupture process of the 2016, M_w6.1 Amatrice earthquake by jointly inverting the most comprehensive dataset to date formed by Strong Motion data, High-Rate sampling Global Positioning System (HRcGPS) data, coseismic offsets derived from continuous and survey GPS networks and Synthetic Aperture Radar Interferometry data (DInSAR) from distinct satellites.
- Study the complexity of the rupture history by means of rupture velocity and rupture mode propagation analyses.
- Investigate the role played by pre-existing tectonic structures in controlling the rupture propagation.

The key idea of our study is that the rupture process of the 2016 Amatrice earthquake has been characterized by a strong geometrical and rheological control due to the fault system segmentation in the central Apennines.

2. Data Sources

2.1 Seismological Data

We have selected 20 strong motion data from stations (Figure1) belonging to the DPC Rete Accelerometrica Nazionale (RAN, http://ran.protezionecivile.it) and to the Rete Sismica Nazionale, Istituto Nazionale di Geofisica e Vulcanologia (RSN, INGV Seismological Data Centre, 1997) accelerometric networks. We also incorporate coseismic dynamic displacements retrieved from High-Rate sampling (from 1 to 0.05 s) continuous Global Positioning System (HRcGPS) data from 6 permanent stations [Avallone et al., 2016] operated by Rete Integrata Nazionale GPS (RING INGV Working Group, 2016;

http://ring.gm.ingv.it). The epicentral distances of the recording sites are less than 70 km, the azimuthal coverage is good and several seismic and GPS stations lie on the hanging wall of the causative fault (Figure1). Original acceleration and displacement recordings are integrated and derived, respectively, to obtain ground velocity time histories. The resulting velocity waveforms are band-pass filtered between 0.02 and 0.5 Hz using a two-pole and two-pass Butterworth filter. We invert 40 seconds of each waveform. In order to efficiently model the wave propagation, the Green's functions are computed, with a discrete wave-number technique [Spudich and Xu, 2003], by considering four different crustal structures, obtained by subdividing the epicentral region in four group stations depending on the azimuth and on the epicentral distance (FigureS1a). For each group we draw mean Vp and Vs 1D profiles (FigureS1b), S1c), respectively), by averaging 8 station-to-epicenter sampling tracks, extracted from the 3D crustal IMAGINE_IT model [Casarotti et al., 2016]. All the P arrivals are corrected with the topography at each site.

2.2 Geodetic Data

We consider a comprehensive geodetic dataset of GPS and Synthetic Aperture Radar Interferometry (DInSAR) displacements. In particular we select 30 coseismic offsets derived from continuous and survey GPS networks operated by INGV, CaGeoNet and Istituto Geografico Militare [Cheloni et al., 2017].

DInSAR data, processed using SARscape® software, consists of two L-band ALOS-2 interferometric pairs from Japan Aerospace Exploration Agency (JAXA), acquired in ascending and descending geometries, and one descending X-band COSMO-SkyMed (CSK) pair, from Italian Space Agency (ASI). Two C-band Sentinel-1 pairs, from European Space Agency (ESA), in ascending and descending geometries are also available. ALOS-2 and Sentinel-1 are in good agreement, but Sentinel-1 maps show lower data coverage due to the sensor wavelength [Bignami et al., 2016; Cheloni et al., 2017]. Thus, we use the two ALOS-2 and the CSK datasets. ALOS-2 dataset highlights fringe patterns characterized by two main lobes (every fringe corresponds to 12 cm of displacement), and with a maximum displacement of -28 cm in Line of Sight (LoS), where negative values are moving away from the satellite (FigureS2). CSK fringes show similar patterns with maximum values of -25 cm;

due to the relatively shorter (3.1 cm) wavelength, CSK is more sensitive to the vegetation, causing loss of coherence of the signal. For an exhaustive description of all datasets, see previous SAR based works [Bignami et al., 2016; Lavecchia et al., 2016; Cheloni et al., 2017; Huang et al., 2017]. Displacement maps are subsampled at 500 m spacing in the maximum deforming areas and 1000 m around them, obtaining about 1400 points for each ALOS-2 dataset and 900 points for CSK.

We compute the Green's functions on the fault plane by adopting a stratified velocity model obtained by averaging the four Vp and Vs 1D profiles (FigureS1b)-c)).

2.3 The fault model set up

Separate geodetic and joint inversions have been performed by adopting TDMT focal mechanism solution (http://cnt.rm.ingv.it/event/7073641/?tab=MeccanismoFocale-TDMTinfo). In all cases, we retrieve models not consistent with the observed interferometric data, i.e. the inverted deformation field largely underfits the observed one, especially at the outbreak of the fault. In order to fit both geodetic and seismological observations, we build-up a fault plane striking N164°E (consistent with the strike angle well constrained by geodetic data [Cheloni et al., 2017], magenta planes in FigureS3) and dipping 50° to the SW. The adopted hypocentre, located at 13.238°E, 42.704°N, at a depth of 6.3 km (red star in FigureS3) is in full agreement with the hypocentre relocated by Chiarabba et al. [2018] (blue star in FigureS3).

3. The Rupture Process of the 2016 Amatrice Earthquake

We consider a fault plane 30.8 km long and 15.4 km wide, divided into squared subfaults (1.925 km length). The model parameters (peak slip velocity, slip direction, rupture time and rise time) are assigned at the corners of each subfault and their values bilinearly interpolated inside of it. Each point on the fault can slip only once, starting at the time of the rupture onset and stopping after the rise time duration, following a prescribed source time function: here we use a dynamically consistent regularized Yoffe function [Tinti et al., 2005], characterized by T_{acc} (the time duration from the rupture onset to the peak slip velocity) equal to 0.225s.

All kinematic parameters are simultaneously inverted by adopting the following ranges: peak slip velocity between 0 and 3.5 m/s at 0.25 m/s interval; rise time between 0.75 and 3 sec at 0.25 sec interval and rake angle, with which we represent the slip direction, between -115° and -55° at 5° interval. The rupture time at each grid node is constrained by the arrival time of a rupture front from the hypocentre having a speed comprised between 1.4 and 4 km/s.

We use a nonlinear inversion method, based on the heat-bath simulated annealing algorithm, which is able to jointly invert strong ground motions records and geodetic data [Piatanesi et al., 2007; Cirella et al., 2012].

Figure2 shows our preferred rupture model in terms of total slip, slip direction, rise time and rupture onset time. We obtain this model by averaging all models belonging to a subset of the model ensemble produced during the search for the best. This subset is populated by those models having a cost function not higher than 5% of the minimum value of the cost function of the best model (about 17000 out of 1.6 millions of models). The averaged model is smoother and more blurred than the best: nevertheless, similar to previous papers [Piatanesi et al., 2007; Cirella et al., 2008], and as reported in Supporting Information (FigureS4, TableS1, TableS2), the stable features of the rupture process are robustly retained by the average model. The preferred model of Figure2 is also able to predict well the observations: Figure3 shows the fit to DInSAR data for ascending, descending ALOS-2 and CSK satellites (panels a)-b)-c), respectively); Figure4b) displays the fit to GPS horizontal and vertical displacements; Figure4a) displays the fit to filtered ground velocity time histories. The joint inversion yields a rupture model containing all the key features of the models retrieved from separate geodetic and seismic inversions (FigureS6).

The main outcome emerging from our modelling is the evident complexity of the rupture process, which is particularly intriguing with respect to the moderate magnitude of the earthquake. To the first order, the earthquake is characterized by a prominent bilateral rupture, with two distinct patches of slip located SE and NW of the hypocentre. The SE patch has 0.7 m of maximum slip and consists in a region of about 8km^2 slipping more than 0.5 m; the NW patch, quite larger than the previous one, reaches 1.3 m of maximum slip with a fault region of about 35km^2 slipping more than 0.5 m. The obtained seismic moment is M_0=1.89 × 10^{18} Nm, corresponding to a M_w6.1; roughly, the SE and NW patches release 35% (0.66×10^{18} Nm)

and 65% (1.23×10^{18} Nm) of the total seismic moment, respectively. The hypocentral area, where the rupture nucleates, features very low slip (less than 0.1m).

The slip direction reveals a dominant normal mechanism with a very small left-lateral strike slip component, the rake angle being quite uniform along the fault plane and ranging between -80° and -85°.

The rise time distribution roughly correlates with the slip pattern, but we observe that the largest rise time (2.2 s) occurs in the shallowest part of the SE patch and does not coincide with the largest slip: this means that the NW patch ruptured at higher slip velocity than the SE patch (Figure2c).

The position of the rupture front on the fault plane (robustly retrieved from the kinematic inversion (FigureS5)) allows us to calculate the rupture velocity vectors at each node [Cirella et al., 2012]. Figure2c) shows the distribution of the rupture velocity amplitude and vector (black arrows) on the fault plane, overlapped by the slip distribution (black contour lines); the rupture velocity is very heterogeneous, reaching 3.2 km/sec along the strike direction in a region between 4km and 8km NW from the hypocentre, corresponding to the main slip patch. The slip patch located to SE from the nucleation, affecting the epicentral region between Accumoli and Amatrice, shows a lower and mostly homogeneous rupture velocity (~2.3km/sec). The rupture velocity vectors feature a rupture front rotation associated with the rupture front acceleration in the focusing region on the path labelled from point R to R' (Figure2a)-c)). This result is supported by the analysis of the relationship between the rupture mode and the rupture velocity, based on the computation of the rupture mode index (RMI) that, as defined by Pulido & Dalguer [2009], is proportional to the angle between the slip direction and the rupture propagation direction. In Figure2d) we plot the values of RMI across the 2016 Amatrice fault plane; values close to 1 and 0 correspond to a pure mode II (in-plane) rupture and to a pure mode III (anti-plane) rupture, respectively. We observe that the rupture propagates in mode II along a narrow downdip area around the hypocentre, in mode III in regions of the fault plane adjacent to the nucleation slipping more than 0.5 m and where the fault ruptures bilaterally along the strike direction; while a transition from mode III to mode II occurs along the path from point R to R', where the rupture front rotates. In order to better illustrate this interesting feature of the rupture propagation, we show in Figure2e) some

snapshots of the slip velocity taken at 0.5 s interval (MovieS1). The first 3 seconds are characterized by bilateral rupture propagation, with no slip at nucleation; then, the rupture starts breaking the higher slip concentration, propagating with a relatively high rupture velocity (~3.0-3.2 km/s) in the NW direction (lasting nearly 1 second). At nearly 4s, the rupture of the northern asperity shows a very peculiar behaviour: the propagation of the pulse seems to be impeded ahead of the current direction and splits into two pulses; along the updip direction and along nearly 32° in the downdip direction.

4. Discussion and Conclusive Remarks

The main contribution of our work is to provide a robust and detailed source model of the first shock of the 2016 Central Italy seismic sequence, well constrained by the use of the available data collected around 2 years after the event. Our analysis confirms previous findings, such as the prominent bi-lateral rupture [Tinti et al., 2016; Lavecchia et al., 2016; Cheloni et al., 2017; Huang et al., 2017; Chen et al., 2018], with low to no slip at the hypocentre and two well separated slip patches, with maximum slip (nearly 1.3m) on the NW patch; and the largely variable rupture velocity, between 2.2 – 3.2km/s, in agreement with Liu et al. [2017]. The northern asperity features very shallow slip, indicating a coseismic activation of the fault along the western flank of the Mount Vettore, as suggested by Cheloni et al. [2017]. However, our model reveals additional peculiar behaviour, such as the acceleration of the rupture front up to 3.2 km/s and the relatively short rise time when breaking the main slip patch, thus indicating an impulsive rupture process there. Furthermore, our model unveils an intriguing behaviour in the northern fault zone, just after the breakage of the main NW slip patch, when the rupture abruptly split in two pulses, towards updip and nearly 32° along the downdip direction.

This feature seems to be in agreement with the presence of a structural and stress barrier controlling the entire seismic sequence evolution, as proposed by previous studies [Pizzi et al., 2017; Mildon et al., 2017; Chiaraluce et al., 2017]. In order to characterize the geometry of this barrier, we compare our fault model with the aftershock hypocentres relocated by Chiaraluce et al. [2017], the mapped fault traces [Civico et al., 2018; Villani et al., 2018] and Vp and Poisson ratio tomographic model obtained by Chiarabba et al. [2018]. The aftershocks

alignment identifies a 190° striking and 32° dipping plane emerging in correspondence to the STF (Figure5a-5b, FigureS7). This plane intersects our fault in correspondence of the splitting zone identified by the rupture evolution (Figure2e). Comparing the imaged slip distribution with the Vp values along the fault plane (Figure5c), we observe that Vp' values increase moving from the high slip zone to north crossing the identified plane (dashed line in Figure5c), highlighting the presence of a bulge/up-warp geometry compatible with a thrust-and-fold structure [Chiarabba et al., 2018]. Moreover, we observe that the zone of transition with enhanced Poisson ratio values (see blue mapped colour in Figure5d) coincides with the fault area where the along-strike rupture propagation has been impeded and split. As suggested by Cirella et al. [2012], this feature involves the role of heterogeneity of material properties, which might result in heterogeneous rheological properties driving the rupture history. It is worth noting the low Poisson ratio value associated with the southern slip patch, where our model shows a low and mainly homogeneous rupture velocity. This feature is coherent with the observation that stations located in the NW region of the source show relatively larger ground accelerations than those located to the SE, with PGA values ranging from 0.45g to 0.02g [Spagnuolo et al., 2016].

All these evidences corroborate the hypothesis that the rupture evolution of the 2016 Amatrice earthquake has been strongly controlled by the presence of a tectonic structure, acting as a geometrical and rheological barrier; its location, trace, strike and dip could be associated with the lateral ramp of the STF. This interpretation is in agreement with the results obtained by Pizzi et al. [2017]. Scognamiglio et al. [2018], propose a kinematic model for the October events, in which a complex rupture is distributed along two faults: the BVFS and a secondary one, identified as the STF. Thus, the same structure acting as barrier during the August 24th shock has been likely activated in the subsequent evolution of the sequence. As those authors suggested, a detailed description of the rupture velocity features, as done in our study, is a key issue to evaluate the role of the fault segmentation.

Cross structures may act as barriers to rupture and limit earthquake length [Manighetti et al., 2015; Benedetti, 2013], with critical consequences to seismic hazard assessment [DuRoss et al., 2016].

Our results provide a complete description of the rupture propagation and inhibition due to spatial distribution of rheological heterogeneities and to the presence of inherited tectonic structures. Their role in the seismic sequence evolution depends on their orientation with respect to the current stress field. In this context, the interaction between new and/or inherited faults, derived from either the Mesozoic extension or the Miocene compression, strongly influences the fault segmentation and fault lengths, determining the maximum magnitude of individual earthquakes [e.g. Wells and Coppersmith, 1994] and consequently the seismic hazard.

Acknowledgments.

We thank Pasquale De Gori, Federica Magnoni, Claudio Chiarabba, Luigi Improta, Simone Atzori for helpful discussion. Data used are available at ESM-Engineering Strong-Motion database (http://esm.mi.ingv.it/). Sentinel-1, ALOS-2, CSK data are copyright of Copernicus (2016), JAXA (AO-P1101002, 2016) and ASI (dedicated acquisition plan, 2016), respectively.

References

Avallone, A., D. Latorre, E. Serpelloni, A. Cavaliere, A. Herrero, G. Cecere, et al. (2016), Coseismic displacement waveforms for the 2016 August 24 Mw 6.0 Amatrice earthquake (central Italy) carried out from High-Rate GPS data, *Ann. Geophys.*, 59 (Fast Track 5), https://doi.org/10.4401/ag-7275.

Barchi, M., DeFeyter, A., Magnani, B., Minelli, G., Pialli, G., & Sotera, B. (1998a). The structural style of the Umbria-Marche fold and thrust belt. *Memorie della Società Geologica Italiana*, 52, 557–578.

Barchi, M., DeFeyter, A., Magnani, M., Minelli, G., Pialli, G., & Sotera, B. (1998b). Extensional tectonics in the Northern Apennines (Italy): Evidence from the CROP03 deep seismic reflection line. *Memorie della Società Geologica Italiana*, 52, 528–538.

Benedetti, L., Manighetti, I., Gaudemer, Y., Finkel, R., Malavieille, J., Pou, K., Keddadouche, K. (2013). Earthquake synchrony and clustering on Fucino faults (Central Italy) as revealed from in situ ^{36}Cl exposure dating, *J. Geophys. Res.*, 118, 4948–4974. https://doi.org/10.1002/jgrb.50299

Bignami, C., C. Tomolei, G. Pezzo, F. Guglielmino, S. Atzori, E. Trasatti, A. Antonioli, S. Stramondo, and S. Salvi (2016), Source identification for situational awareness of August 24th 2016 central Italy event, *Ann. Geophys.*, 59 (Fast Track 5), https://doi.org/10.4401/ag-7233.

Butler, R. W., Tavarnelli, E., & Grasso, M. (2006). Structural inheritance in mountain belts: An Alpine–Apennine perspective. *Journal of Structural Geology*, 28(11), 1893–1908.

Casarotti, E., F. Magnoni, L. Faenza, F. Comunello, P. Polidoro, and S. Mulargia (2016), Fast 3D Seismic Wave Simulations of 24 August 2016 M_w 6.0 Central Italy Earthquake for Visual Communication, *Ann. Geophys.*, 59 (Fast Track 5), https://doi.org/10.4401/ag-7231.

Cavinato, G. P., & De Celles, P. G. (1999). Extensional basins in the tectonically bimodal central Apennines fold-thrust belt, Italy: Response to corner flow above a subducting slab in retrograde motion, *Geology*, 27(10), 955–958.

Centamore, E., Rossi, D., & Tavarnelli, E. (2009). Geometry and kinematics of Triassic-to-Recent structures in the Northern-Central Apennines: A review and an original working hypothesis, *Bollettino della Societa Geologica Italiana*, 128(2), 419–432.

Cheloni, D., De Novellis, V., Albano, M., Antonioli, A., Anzidei, M., Atzori, S., et al. (2017). Geodetic model of the 2016 Central Italy earthquake sequence inferred from InSAR and GPS data, *Geophys. Res. Lett.*, 44, 6778–6787. https://doi.org/10.1002/2017GL073580

Chen, K., Liu,Z., Liang,C., and Y.Tony Song (2018), Towards the application of seismogeodesy in central Italy: a case study for the 2016 August 24 Mw6.1 Italy earthquake modelling, *Geophys. J. Int.*, 213, 1647-1658, doi:10.1093/gji/ggy089.

Chiarabba, C., De Gori, P., Cattaneo, M., Spallarossa, D., & Segou, M. (2018). Faults geometry and the role of fluids in the 2016 -2017 Central Ita
Geophys. Res. Lett., 45. https://doi.org/10.1029/2018GL077485

Chiaraluce, L., Di Stefano, R., Tinti, E., Scognamiglio, L., Michele, M., Casarotti, E., et al. (2017). The 2016 Central Italy seismic sequence: A first look at the mainshocks, aftershocks, and source models, *Seism. Res. Lett.*, 88(3). https://doi.org/10.1785/0220160221

Ciarapica, G., & Passeri, L. (2002). The palaeogeographic duplicity of the Apennines. *Bollettino della Societa Geologica Italiana*, 121(1), 67–75.

Cirella, A., Piatanesi, A., Tinti, E. & Cocco, M., (2008). Rupture process of the 2007 Niigata-ken Chuetsu-oki earthquake by non-linear joint inver- sion of strong motion and GPS data, *Geophys. Res. Lett.*, 35, L16306, doi:10.1029/2008GL034756.

Cirella A., Piatanesi A., Tinti E. Chini M. and M. Cocco, (2012), Complexity of the rupture process during the 2009 L'Aquila, Italy, earthquake, *Geophys. J. Int.* , 190, 607-621, doi:10.1111/j.1365-246X.2012.05505.x.

Civico, R., Pucci, S., Villani, F., Pizzimenti, L., De Martini, P. M., Nappi, R., & the Open Emergeo Working Group (2018). Surface ruptures following the 30 October 2016 Mw 6.5 Norcia earthquake, central Italy. *Journal of Maps*, 14(2), 151–160. https://doi.org/10.1080/17445647.2018.1441756

D'Agostino, N., Mantenuto, S., D'Anastasio, E., Avallone, A., Barchi, M., Collettini, C., et al. (2009). Contemporary crustal extension in the Umbria–Marche Apennines from regional CGPS networks and comparison between geodetic and seismic deformation. *Tectonophysics*, 476(1), 3–12.

DuRoss, C. B., Personius, S. F., Crone, A. J., Olig, S. S., Hylland, M. D., Lund, W. R., & Schwartz, D. P. (2016). Fault segmentation: New concepts from the Wasatch fault zone, Utah, USA. *J. Geophys. Res.*, 121, 1131–1157. https://doi.org/10.1002/2015JB012519

Huang, M.-H., E.J. Fielding, C. Liang, P. Milillo, D. Bekaert, D. Dreger, and J. Salzer (2017), Coseismic deformation and triggered landslides of the M_w 6.2 Amatrice earthquake in Italy, *Geophys. Res. Lett*., 44, 1266–1274, doi:10.1002/2016GL071687.

Jarvis, A., H.I. Reuter, A. Nelson, E. Guevara, 2008, Hole-filled SRTM for the globe Version 4, available from the CGIAR-CSI SRTM 90m Database (http://srtm.csi.cgiar.org).

Lavecchia, G. (1985). II sovrascorrimento dei Monti Sibillini: analisi cinematica e strutturale. *Bollettino della Societa Geologica Italiana*, 104, 161–194.

Lavecchia, G., Brozzetti, F., Barchi, M., Menichetti, M., & Keller, J. V. (1994). Seismotectonic zoning in east-central Italy deduced from an analysis of the Neogene to present deformations and related stress fields. *Geological Society of America Bulletin*, 106(9), 1107–1120.

Lavecchia, G., Castaldo, R., de Nardis, R., De Novellis, V., Ferrarini, F., Pepe, S., et al. (2016). Ground deformation and source geometry of the 24 August 2016 Amatrice earthquake (Central Italy) investigated through analytical and numerical modeling of DInSAR measurements and structural-geological data. *Geophys. Res. Lett*, 43, 12,389–12,398. https://doi.org/10.1002/2016GL071723

Liu, C., Y. Zhengm Z. Xie, and X. Xiong (2017), Ruptures features of the M_w 6.2 Norcia earthquake and its possible relationship with strong seismic hazards, *Geophys. Res. Lett*., 44, 1320–1328, doi:10.1002/2016GL071958.

Manighetti, I., Caulet, C., De Barros, D., Perrin, C., Cappa, F., & Gaudemer, Y. (2015). Generic along-strike segmentation of Afar normal faults, East Africa: Implications on fault growth and stress heterogeneity on seismogenic fault planes. *Geochemistry, Geophysics, Geosystems*, 16, 443–467. https://doi.org/10.1002/2014GC005691

Mildon, Z., Roberts, G., Walker, J. F., & Iezzi, F. (2017), Coulomb stress transfer and fault interaction over millennia on non-planar active normal faults: the Mw 6.5-5.0 seismic sequence of 2016-2017, central Italy. https://doi.org/10.1093/gji/ggx213

Piatanesi, A., A. Cirella, P. Spudich, and M. Cocco (2007), A global search inversion for earthquake kinematic rupture history: Application to the 2000 western Tottori, Japan earthquake, *J. Geophys. Res*., 112, B07314,doi:10.1029/2006JB004821.

Pizzi, A., Di Domenica, A., Gallovič, F., Luzi, L., & Puglia, R. (2017). Fault segmentation as constraint to the occurrence of the main shocks of the 2016 Central Italy seismic sequence. *Tectonics*, 36, 2370–2387. https://doi.org/10.1002/2017TC004652

Pulido, N. and L. Dalguer, (2009), Estimation of the high-frequency radiation of the 2000 Tottori (Japan) earthquake based on a dynamic model of fault rupture: application to the strong ground motion simulation, *Bull. Seism. Soc. Am*., 99 (4), 2305-2322,doi: 10.1785/0120080165.

Scognamiglio, L., Tinti, E., Casarotti, E., Pucci, S., Villani, F., Cocco, M., et al. (2018). Complex fault geometry and rupture dynamics of the M_W 6.5, 30 October 2016, central Italy earthquake. *Journal of Geophysical Research: Solid Earth*, 123, 2943–2964.

Spagnuolo E., Cirella, A., Akinci, A., (2016), Investigating the effectiveness of rupture directivity during the August 24, 2016 Mw 6.0 central Italy earthquake, Annals of Geophysics, [S.l.], dec. 2016. ISSN 2037-416X. doi:http://dx.doi.org/10.4401/ag-7213

Spudich, P. and L. Xu (2003), Software for calculating earthquake ground motions from finite faults in vertically varying media, in International Handbook of Earthquake and Engineering Seismology, Academic Press.

Tinti, E., Fukuyama, E., Piatanesi, A. & Cocco, M., (2005). A kinematic source time function compatible with earthquake dynamics, *Bull. Seism. Soc. Am.*, 95(4), 1211–1223, doi:10.1785/0120040177.

Tinti, E., L. Scognamiglio, A. Michelini, and M. Cocco, (2016), Slip heterogeneity and directivity of the ML6.0, 2016, Amatrice earthquake estimated with rapid finite fault inversion, *Geophys. Res. Lett.*, 43, 10, 745-752, doi: 10.1002/2016GL071263

Vezzani, L., Festa, A., & Ghisetti, F. C. (2010). Geology and tectonic evolution of the Central-Southern Apennines, Italy. *Geological Society of America Special Papers*, 469, 1–58.

Villani, F., Civico, R., Pucci, S., Pizzimenti, L., Nappi, R., De Martini, P. M., & the Open EMERGEO Working Group (2018). A database of the coseismic effects following the 30 October 2016 Norcia earthquake in Central Italy. *Science Data*, 5, 180049. https://doi.org/10.1038/sdata.2018.49

Donald L. Wells, Kevin J. Coppersmith, (1994), New empirical relationships among magnitude, rupture length, rupture width, rupture area, and surface displacement. *Bull. Seism. Soc. Am.*, 84 (4): 974–1002.

Figures

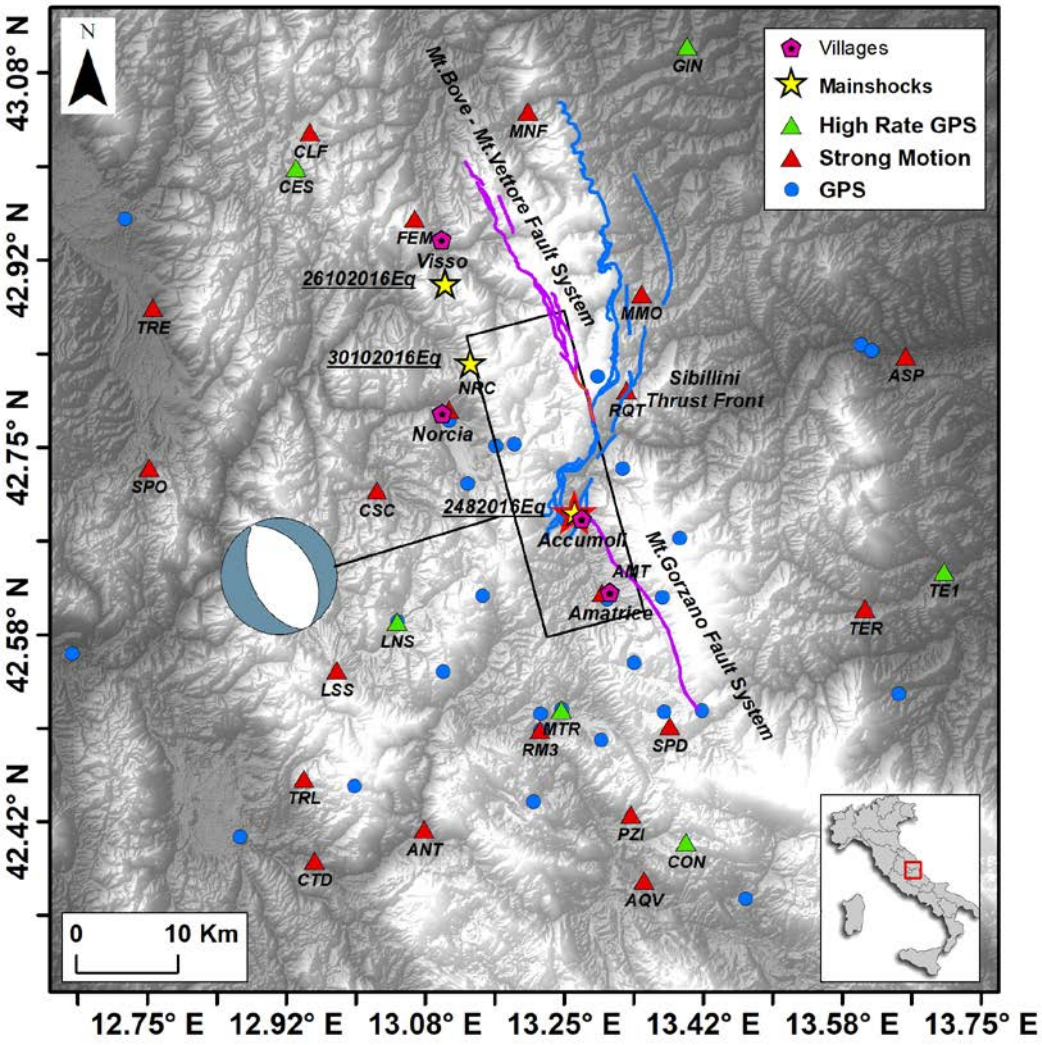

Figure1. Fault geometry of the 2016 Amatrice, central Italy, earthquake. Red and green triangles represent the strong motions and the HRcGPS stations. Blue circles are the GPS sites. The red star indicates the epicenter. Black box represent the surface projection of the fault plane. Purple and cyan lines are the GFS-BVFS and the STF, respectively.

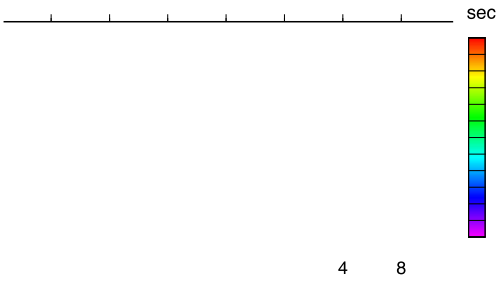

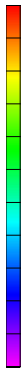

Figure2. Inverted rupture model. Panels a)-b) show the total slip and the rise time, respectively. Rupture time shown by black contour lines (in seconds); black arrows displayed in upper plot represent the slip vector. c) Rupture velocity amplitude and vectors across the

fault plane; d) rupture index across the fault plane; e) time snapshots of slip velocity on the fault plane, imaged every 0.5 sec. Black contours in c) and d) and white contours in e) both show the regions that slipped more than 0.1 m, 0.5 m and 1.0 m. White and red star displays the hypocentre.

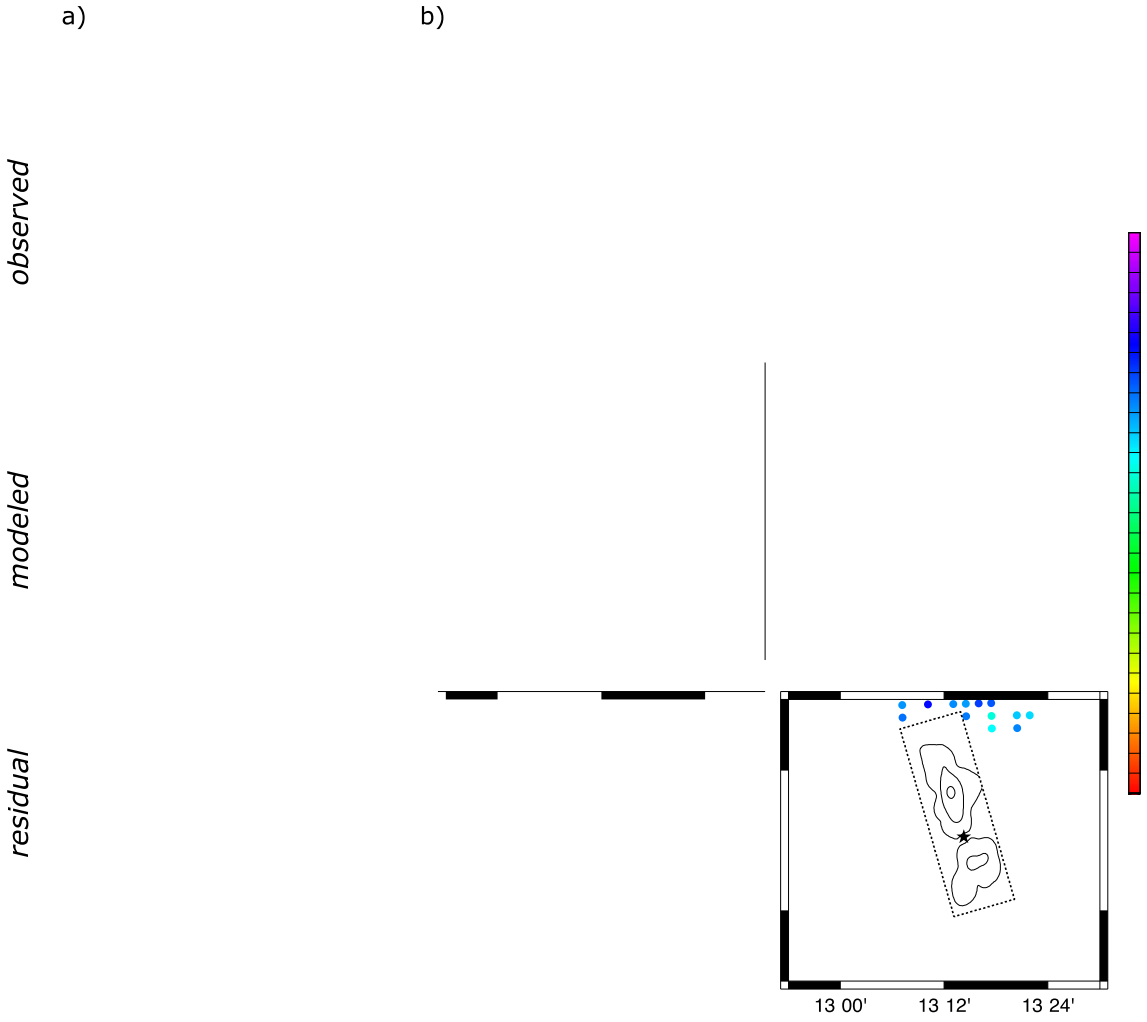

Figure3. Observed, synthetic DInSAR displacements and their residuals (upper, middle and bottom panels, respectively), observed from ascending track ALOS-2 (panel a); descending track ALOS-2 (panel b); and CSK (panel c) satellites. Dashed black box represents the surface projection of the fault plane. Black contour lines display the slip distribution. Black star displays the hypocentre.

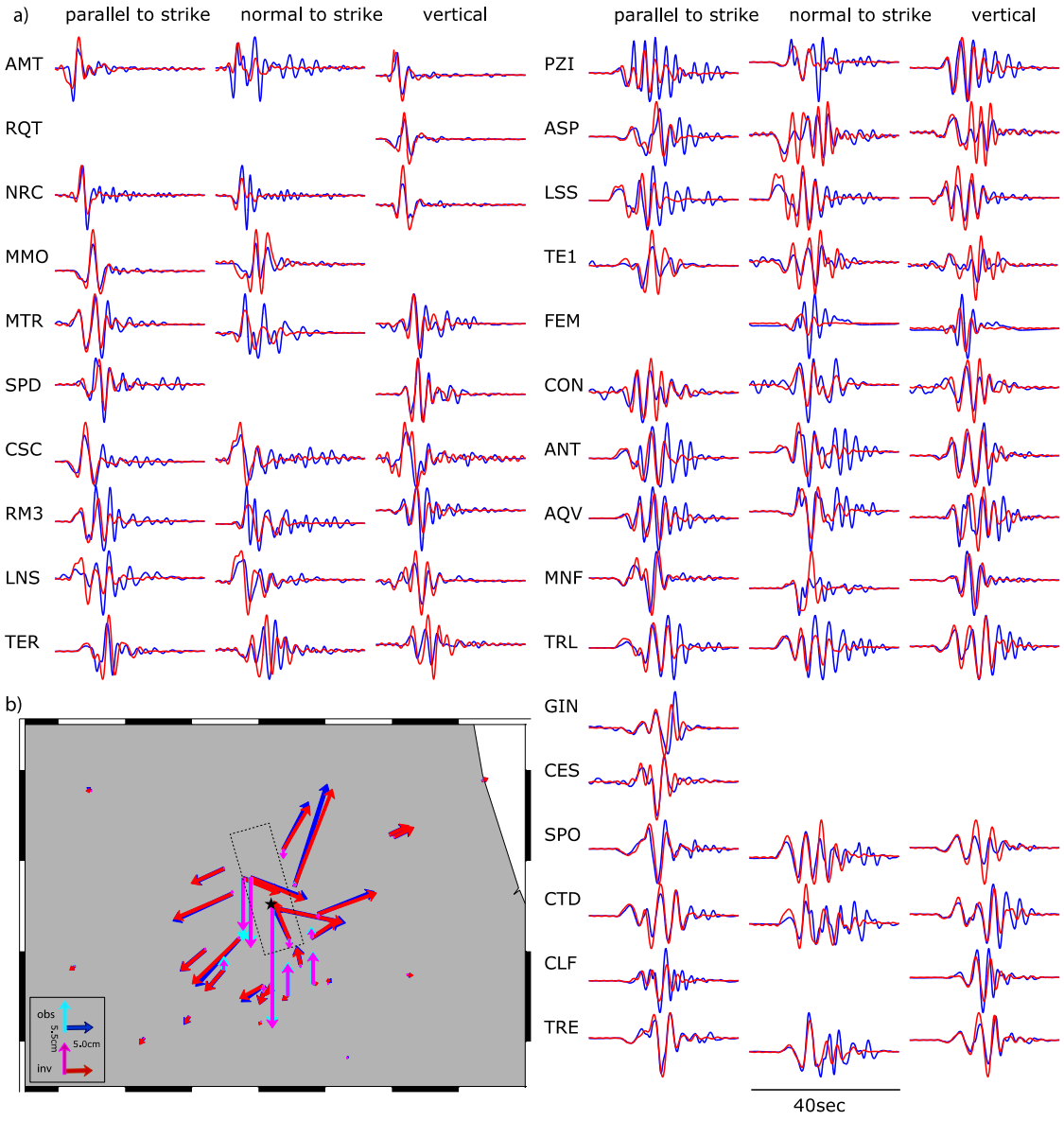

Figure4. a) Comparison of recorded strong motion and HRcGPS (blue lines) with synthetic waveforms (red lines); b) comparison of measured (blue and cyan arrows) with synthetic (red and violet arrows) horizontal and vertical (respectively) coseismic displacements.

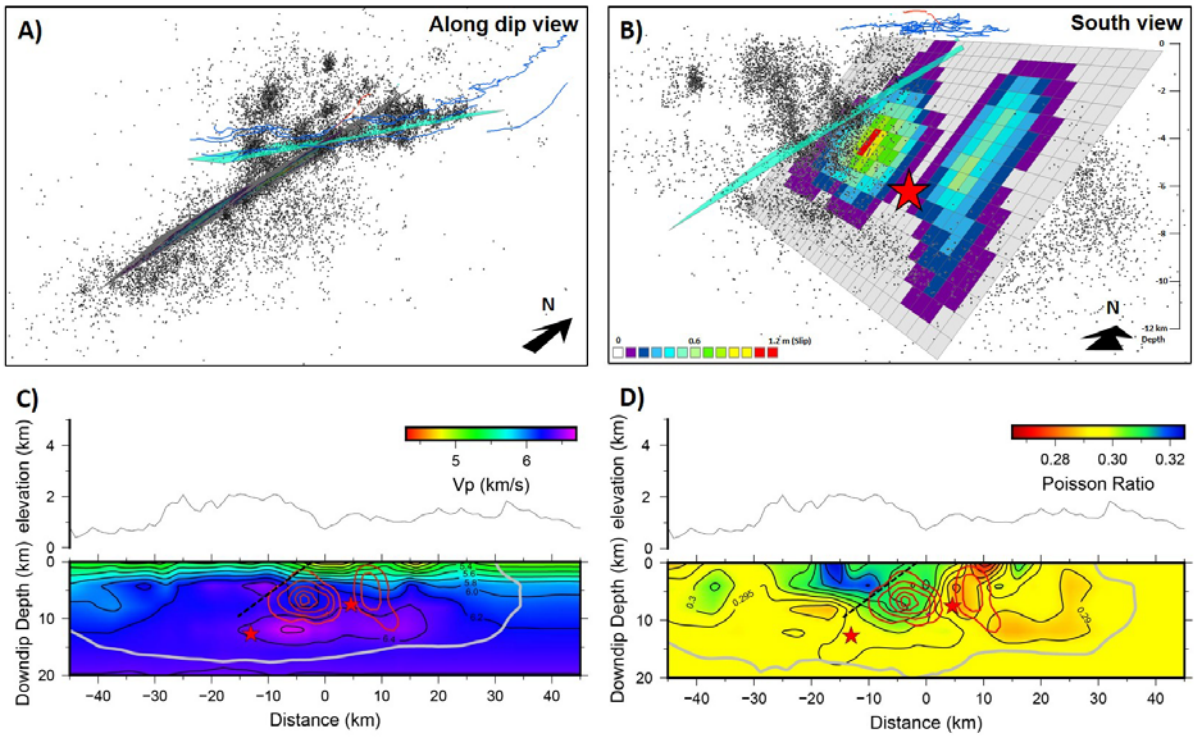

Figure5. a) and b) 3D views of the modelled fault with the STF(cyan plane) and seismicity. The thrust and normal fault traces (in blue and red, respectively). c) Vp and d) Poisson ratio projected along the fault plane, with 20 cm spacing contours of the modelled slip (in red); the thrust and fault intersection (dashed black line); and M_w > 5.0 shocks; the resolved zone within grey contour. Purple and cyan lines are the GFS-BVFS and the STF, respectively. Elevation data from Jarvis et al. [2008].